# EFFECT OF PARAMETERS ON THERMAL AND FLUID-FLOW BEHAVIOR OF BATTERY THERMAL MANAGEMENT SYSTEM

by

***Asif AFZAL[a*], Awatef ABIDI[b,c,d], Mohammed Samee AD[e], Abdul Razak RK[a], Manzoore Elahi M. SOUDAGAR[f], and Ahamed Saleel C[g]***

[a] Department of Mechanical Engineering, P. A. College of Engineering, (Affiliated to Visvesvaraya Technological University, Belagavi), Mangaluru, India
[b] Physics Department, College of Sciences Abha, King Khalid University, Abha, Saudi Arabia
[c] Research Laboratory of Metrology and Energy Systems, National Engineering School, Energy Engineering Department, Monastir University, Monastir City, Tunisia
[d] Higher School of Sciences and Technology of Hammam Sousse, Sousse University, Sousse, Tunisia
[e] Department of Mechanical Engineering, N.K.Orchid College of Engineering and Technology, Solapur, Maharashtra, India
[f] Department of Mechanical Engineering, Glocal University, Delhi-Yamunotri Marg, SH-57, Mirzapur Pole, Saharanpur District, Uttar Pradesh, India
[g] Department of Mechanical Engineering, College of Engineering, King Khalid University, Abha, Kingdom of Saudi Arabia

Original scientific paper
https://doi.org/10.2298/TSCI191206290A

*In modern electric vehicles the thermal stability problems associated with Lithium-ion battery system is of major concern. Proper battery thermal management systems is required to ensure safety and efficient performance of battery cells. A realistic conjugate heat transfer and fluid-flow analysis of Lithium-ion prismatic battery cell is performed. The flow of air as coolant, is laminar, flowing between the heat generating battery cells. The effect of few important working parameters like volumetric heat generation, $\overline{S}_q$, conduction-convection parameter, $\zeta_{cc}$, Reynolds number, aspect ratio, Ar, and spacing between the cells, $\overline{W}_f$, is investigated in this work. For the wide range of parameters considered, the temperature variations in battery cell and coolant is carried out. Focusing mainly on effect of Reynolds number and $\overline{W}_f$, behavior of local Nusselt number, local friction coefficient, $C_{f,x}$, average Nusselt number, average friction coefficient, $C_{f,avg}$, maximum temperature, mean fluid temperature, heat removed from the lateral surface of cell are discussed. Average Nusselt number increased with increase in Reynolds number but decreased with increase in $\overline{W}_f$, whereas $C_{f,avg}$ decreased with increase in Reynolds number and $\overline{W}_f$. It is also found that their exists an upper and lower limit on Reynolds number and $\overline{W}_f$ above and below which the change in $C_{f,avg}$ and average Nusselt number is negligible. Maximum temperature is significantly influenced at low Reynolds number and for all $\overline{W}_f$. From the lateral surface of battery over which the coolant flows, more than 96% of heat generated in cell is removed.*

Key words: *Nusselt number, friction coefficient, spacing, battery cell, heat generation, thermal behavior, Reynolds number*

* Corresponding author, e-mail: asif.afzal86@gmail.com

## Introduction

Recent development in automobile technology has given the most reliable and clean source of energy in the form of electrochemical energy [1-3]. Lithium ion (Li-ion) batteries are the most widely used source of electrochemical form of energy. But again, this source of electrochemical energy requires better thermal management system, so that it can operate safely without creating damage to the devices and vehicles in which it is being used [4-6]. Thermal management of heat generating Li-ion batteries plays a vital role for improved performance, high efficiency, long service life and safer operation. If the heat generated in the battery cell is not removed appropriately, additional heat-generating exothermic reactions are triggered by the temperature rise. This results in an increased temperature of the battery cell which causes a thermal runaway situation. Therefore, the heat generated in the battery cell should be adequately removed, adopting an effective cooling mechanism [7, 8].

Heat transfer characteristic of 3-D battery cell was demonstrated with some suitable cooling method. Baker and Verbrugge [9] proposed a 2-D model of Li-ion battery cell to study the causes for thermal runaway. In this study they mainly focused on determining the strength and location of maximum temperature in a battery cell body during the process of discharging and charging. Ramadass *et al.* [10] performed capacity fade analysis of Sony 18650 Li-ion battery cell. Capacity fade of 30% and 36% were obtained at room temperature and 45 °C, respectively. After 490 cycles, capacity fade of 70% was obtained at 70 °C. They concluded that, increase in temperature affects the capacity fading of Battery cells. Mahamud and Park [11] performed thermal management analysis of cylindrical Li-ion cells with reciprocating air-flow. Lumped capacitance model was considered for the analysis of Li-ion cells assuming uniform heat losses. Results obtained show that reciprocating air-flow arrangement reduces maximum temperature by 1.5 °C. Tran *et al.* [12] used the combined method of heat pipe cooling of battery module for better thermal performance and high efficiency. Natural-convection effects are insufficient to maintain the temperature of battery within the operating range. Combination of heat pipes along with ventilation provided better thermal management of battery cells [13, 14].

Rao *et al.* [15] investigated a cooling method for battery system in which they used coupled technique of PCM and mini-channels. The obtained results from this study suggest that the combined effects of PCM mini-channels give more satisfactory results as compared to PCM alone. Chen *et al.* [16] compared four different methods, direct air cooling, direct liquid cooling, indirect liquid cooling and fin cooling of battery pack having Li-ion cells. The best and optimal method is suggested in this 3-D numerical simulation in terms of controlling the maximum range of temperature within the battery pack, temperature uniformity, and power efficiency. Basu *et al.* [17] suggested a correlation for predicting the temperature of each individual cell in a 3-D packed battery module which can eliminate the usage of temperature sensors to greater extent. The study also conclude that the conductivity of a conduction element which acts as a screen between liquid coolant and battery cell plays very prime role in efficient heat transfer. Chalise *et al.* [18] investigated a conjugate heat transfer problem pertinent to liquid cooling of Li-ion battery pack with analytical approach. Different fluid and flow velocity were considered to determine the efficient performance of battery pack. Li *et al.* [19] analyzed thermal behavior of Li-ion battery system cooled by air. Velocity of air up to 30 m/s was considered for analysis and a reduced-order model was developed to predict the maximum temperature in battery module. The operating parameters of battery module and their influence on the thermal and fluid-flow behavior of different battery models have been discussed specifically in the literature [20-23].

Thermal management of battery cells considering some active/passive cooling techniques are commonly reported as seen from the aforementioned literature review. Using commercial software like ANSYS-FLUENT most of the research works were carried to analyze the coolant flow behavior and its arrangement. While the experimental studies mainly focused on charging and discharging effect on thermal behavior of battery cells considering only the solid cell. However, the realistic conjugate condition at the solid battery cell and coolant interface is not reported, except Chalise *et al.* [18]. Chalise *et al.* [18] performed a conjugate analysis of battery cell considering few coolants and flow velocity by analytical method and external flow. Boundary-layer equation was used by Chalise *et al.* [18] to conduct the analytical analysis focusing on maximum temperature and temperature distribution keeping the parallel cell plate far away from the vicinity of considered battery cell. Giving consideration some of the previously stated facts and taking motivation from them, the present investigation is intended to perform a numerical simulation by considering the parametric effect on a realistic conjugate thermal behavior of prismatic battery cell cooled by air. The parameters considered are spacing between cells, $\overline{W}_{\mathrm{f}}$, volumetric heat generation, $\overline{S}_q$, conduction-convection parameter, $\zeta_{\mathrm{cc}}$, Reynolds number, and aspect ratio, $Ar$. Accordingly, an indigenous finite volume method (FVM) based code was developed to perform the analysis. The effect of $\overline{W}_{\mathrm{f}}$ and Reynolds number are given a special attention on the variation of temperature distribution, friction coefficient, Nusselt number, maximum temperature and heat removed from the lateral surface of cell.

## Numerical analysis

### *Physical model*

A parallel channel with liquid coolant flow is employed to cool the battery cells during operation. The developed thermal model is then used to analyze the thermal behavior of the battery cell for various parameters, as shown in fig. 1. The fluid-flow inside the channel is commonly in laminar regime owing to the low velocity of the flow inside the channel. Based on some previous literature survey, the heat generation is assumed uniform [24-26]. The governing equations were solved by considering steady-state as the heat generated during charging or discharging routes taken over a long time is assumed constant.

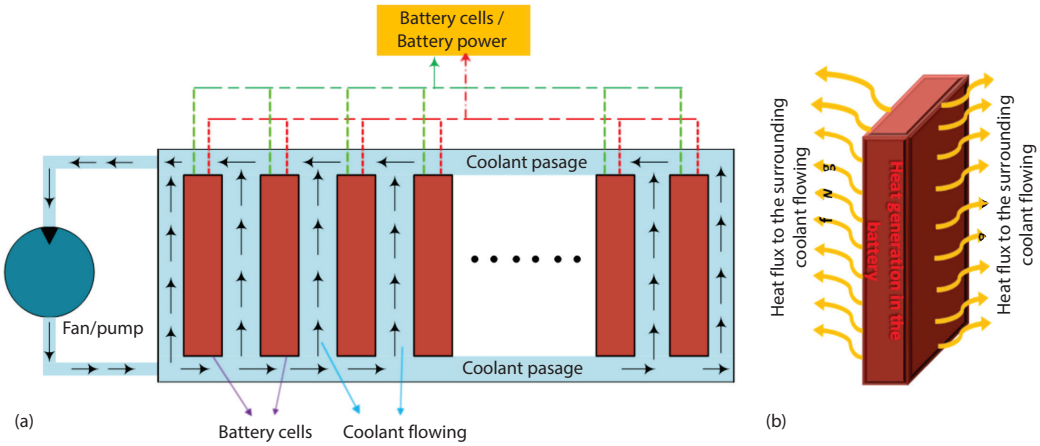


**Figure 1. Schematic view of arrangement of battery cells with air circulation fan and heat generation in batteries; (a) compact battery module with stack of batteries and coolant passages and (b) heat flux from the battery surface**

*Mathematical model*

The governing equations describing the heat transfer process when discharging/charging the Li-ion battery cell is given:

$$k_s \nabla^2 T + q''' = 0 \tag{1}$$

where $q'''$ is volumetric heat generation term.

The governing equations for 2-D, steady, incompressible, laminar, forced convection flow in the fluid domain are continuity equation, $x$ and $y$ momentum equations and equation of energy, which are:

$$\nabla u = 0 \tag{2}$$

$$(u\nabla u) = -\frac{1}{\rho}\nabla p + \mu\nabla^2 u \tag{3}$$

$$u\nabla T = \alpha\nabla^2 T \tag{4}$$

The aforementioned equations are non-dimensionalized using the following set of normalizing parameters:

$$\begin{gathered}\overline{S}_q = \frac{q'''{w_\mathrm{s}}^2}{k_\mathrm{s}(T_o - T_\infty)},\ C = 4Ar^2,\ \overline{T} = \frac{T - T_\infty}{T_o - T_\infty},\ L_i = \frac{l_i}{L},\ L_o = \frac{l_o}{L},\ X = \frac{x}{L} \\ U = \frac{u}{u_\infty},\ V = \frac{v}{u_\infty},\ P = \frac{p}{\rho u_\infty^2},\ Ar = \frac{L}{2w_\mathrm{s}},\ Y_\mathrm{s} = \frac{y_\mathrm{s}}{w_\mathrm{s}},\ Y_\mathrm{f} = 1 + \frac{y_\mathrm{f}}{L} \\ \overline{W}_\mathrm{f} = \frac{w_\mathrm{f}}{L},\ \zeta_\mathrm{cc} = \frac{k_\mathrm{f}}{k_\mathrm{s}}\left[\frac{w_\mathrm{s}}{L}\right],\ \mathrm{Re} = \frac{u_\infty L}{\nu},\ \mathrm{Pr} = \frac{\nu}{\alpha}\end{gathered} \tag{5}$$

The final set of non-dimensionalized governing equations turns out to be:

$$\frac{\partial^2 \overline{T}_\mathrm{s}}{\partial X^2} + C\frac{\partial^2 \overline{T}_\mathrm{s}}{\partial Y_\mathrm{s}^2} + C\overline{S}_q = 0 \tag{6}$$

$$\nabla U = 0 \tag{7}$$

$$U\nabla U = -\nabla P + \frac{1}{\mathrm{Re}}\nabla^2 U \tag{8}$$

$$U\nabla\overline{T_\mathrm{f}} = \frac{1}{\mathrm{RePr}}\nabla^2 T_\mathrm{f} \tag{9}$$

The normalized governing equations given previously are coupled PDE (elliptic in nature) and thus require specification of boundary conditions on all the boundaries. At the inlet, the axial component of the velocity and the inlet temperature distribution are understood to be uniform:

$$X = 0,\quad 0 \le Y_s \le 1,\quad U = 0,\ V = 0,\ \overline{T}_\mathrm{s} = 0$$

At the left side, thermal symmetry boundary condition:

$$Y_\mathrm{s} = 0,\quad 0 \le X \le 1,\quad \partial\overline{T}_s/\partial X = 0$$

At the interface, continuity of temperature boundary condition is used:

$$Y_\mathrm{s} = 1,\quad 0 \le X \le 1,\ \overline{T}_\mathrm{s} = \overline{T}_\mathrm{f}$$

At the top of the domain, heat transfer is assumed to be negligibly small, as at the exit of the cell cathode and anode current collector are present [27]:

$$X = 1, \quad 0 \le Y_s \le 1, \quad \partial \overline{T}_s / \partial Y_s = 0$$

An enlarged extended computational domain of finite section, as shown in fig. 2, has been used in this analysis to mimic the free-stream conditions of the fluid-flow far away from the region of thermal disturbance induced by the battery cells and to capture the diffusive effects of the low Prandtl fluids. Its height is chosen as $l_i$ at the inlet and $l_o$ at the exit, based on a few preliminary studies performed. So the most appropriate boundary condition at the extended domain is:

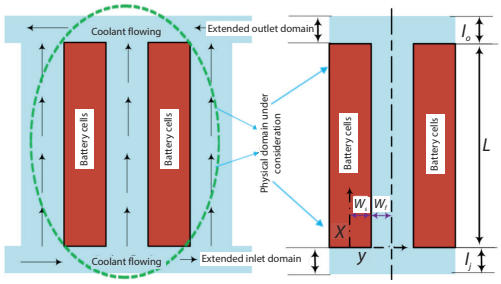


**Figure 2. The symmetric battery (prismatic cell) and coolant flow domain considered for computational analysis**

$$\begin{gathered}
Y_f = 1, \ -L_i \le X \le 0 \ \text{ and } \ L \le X \le L_o, \ \frac{\partial \overline{T}_f}{\partial Y_f} = 0, \ \frac{\partial U}{\partial Y_f} = 0, \ V = 0 \\
Y_f = 1, \ 0 \le X \le L, \ \frac{\partial \overline{T}_f}{\partial Y_f} = \frac{1}{\zeta_{cc}} \frac{\partial T_s}{\partial Y_s}, \ U = 0, \ V = 0 \\
Y_f = 1 + \overline{W}_f, \ -L_i \le X \le (L + L_o), \ \frac{\partial \overline{T}_f}{\partial Y_f} = 0, \ V = 0, \ \frac{\partial U}{\partial Y_f} = 0 \\
X = -Li, \ 1 \le Y_f \le (1 + \overline{W}_f), \ \overline{T}_s = 0, \ U = 1, \ V = 0 \\
X = L + L_o, \ 1 \le Y_f \le (1 + \overline{W}_f), \ \frac{\partial \overline{T}_s}{\partial X} = 0, \ \frac{\partial U}{\partial Y_f} = 0, \ V = 0
\end{gathered} \tag{10}$$

Coolant average Nusselt number, $\mathrm{Nu}_{avg}$, is calculated using eq. (12). Based on Newton's law of cooling at the cell and coolant interface:

$$-k \left. \frac{\partial T}{\partial Y} \right|_{y_s = w_s} = h(T_{y_s = w_s} - T_{f,m}) \tag{11}$$

where $\overline{T}_{f,m}$ is the mean temperature of the fluid domain and $\overline{T}_s$ is the cell surface temperature. Using appropriate dimensionless parameters, the local $\mathrm{Nu}_x$ is obtained which is integrated over the cell surface length to get $\mathrm{Nu}_{avg}$:

$$\mathrm{Nu}_x = -\frac{1}{\left(\overline{T}_{Y_s = W_s} - \overline{T}_{f,m}\right)} \left. \frac{\partial \overline{T}}{\partial Y} \right|_{Y_s = W_s}, \quad \mathrm{Nu}_{avg} = -\int_0^1 \frac{1}{\left(\overline{T}_{Y_s = W_s} - \overline{T}_{f,m}\right)} \left. \frac{\partial \overline{T}}{\partial Y} \right|_{Y_s = W_s} \mathrm{d}X \tag{12}$$

The friction coefficient, $C_f$, variation at the cell and coolant interface along the channel length is estimated based on the Newton's law of viscosity given:

$$\tau_s = \mu \left. \frac{\mathrm{d}u}{\mathrm{d}y} \right|_{y = w_s}$$

According to the practical definition of the shear stress, $\boldsymbol{\tau}_s$, at the surface is given:

$$\boldsymbol{\tau}_s = C_f \frac{\rho u_m^2}{2}$$

Equating the aforementioned equations of $\boldsymbol{\tau}_s$ and using the appropriate non-dimensional terms the following eq. (13) is obtained for local friction coefficient, $C_{f,x}$:

$$C_{f,x} = \frac{2}{\mathrm{Re} U_m^2} \frac{\mathrm{d}U}{\mathrm{d}Y_s}\bigg|_{Y_s=\overline{W}_s} \tag{13}$$

where $U_m$ is the mean velocity of the coolant in the channel. The average friction coefficient, $C_{f,avg}$, is further computed using eq. (14):

$$C_{f,avg} = \frac{2}{\mathrm{Re} U_m^2} \int_0^1 \frac{\mathrm{d}U}{\mathrm{d}Y_s}\bigg|_{Y_s=\overline{W}_s} \mathrm{d}X \tag{14}$$

### *Numerical solution*

The numerical solution of the conjugate problem consisting of energy and momentum equations is obtained by employing staggered grid method of FVM. The SIMPLE algorithm is used to solve the coupled momentum and continuity equation obtain velocity and pressure components. Discretization was done by central differencing scheme for continuity and momentum equations. The diffusion equation of cell domain and energy equation of fluid domain are coupled as the conjugate condition at the cell-fluid interface should be satisfied. Hence they are solved simultaneously using line-by-line gauss seidel method. To evaluate the accuracy of the numerical results, grid-independence tests to check the dependence of the obtained results on the grid resolution was conducted. The considered mesh systems have grid size of 42 × 82, 62 × 122, 82 × 162 in fluid domain and grid size of 82 × 82, 82 × 122, and 122 × 122 in the solid domain, respectively. For typical cases calculated in the present work, the numerical results obtained for non-dimensional temperature for different mesh system was less than 5%. The % deviation for the mesh system tested is mentioned in tab. 1. The % deviation between Mesh 2 and Mesh 3 is lower than between Mesh 1 and Mesh 2. However, to reduce the computational time without affecting the accuracy, a grid size of 62 × 122 for solid domain and fluid domain are used.

**Table 1. Removed heat from the lateral surface for different gird sizes**

| Mesh No. | Mesh 1 | Mesh 2 | Deviation [%] | Mesh 3 | Deviation [%] |
|---|---|---|---|---|---|
| Mesh size | 42×82 | 62×122 | | 82×162 | |
| Heat removed | 0.478451 | 0.484558 | 1.27% | 0.489045 | 0.92 |

### *Validation*

In order to validate the heat transfer and fluid-flow results, the problem has been solved for the external flow problem on nuclear fuel element (Jahangeer *et al.* [28] and Ramis *et al*. [29] which is close to present work available in literature as shown fig. 3, having uniform and non-uniform heat generation term was analyzed. A fairly good agreement was obtained of the temperature distribution between their results and the present FVM code was obtained. The temperature along the width of fuel element for uniform ($\overline{S}_q$ = 0.5 and 0.75) and non-uniform ($\overline{S}_q$ = 0.75) heat generation is plotted. The temperature variation obtained from

the both the work is having the same nature. For uniform heat generation the temperature reduction is smooth along the width. While for axial temperature there is sharp rise reaching to peak and then fall as the top portion of fuel element is reached indicating the non-uniform heat generated at the axial center location. Note that the flow was considered to be external flow with Re = 2500, $Ar$ = 15, and $\zeta_{cc}$ = 0.35.

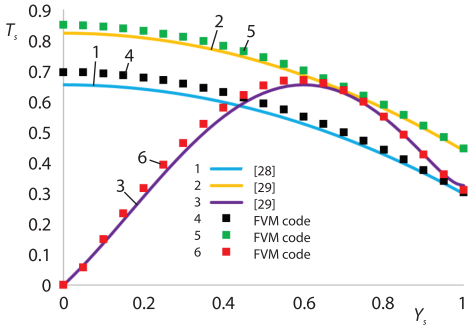


**Figure 3. Present FVM code results in agreement with results from [28] and [29]**

## Results and discussions

### *Effect of parameters on temperature distribution in cell*

The temperature distribution along the transverse direction of cell at center $X$ = 0.5 for change in $\bar{W}_f$ and $\zeta_{cc}$ is shown fig. 4. The temperature is maximum at the center and smoothly reduces and becomes minimum at the surface of cell. The nature of temperature distribution with increase in $\bar{W}_f$ from 0.04-0.14 and $\zeta_{cc}$ = 0.06 is monotonous which is evident from fig. 5(a). When $\bar{W}_f$ is increased from 0.04-0.06, the increase in temperature distribution is least. On further increase in $\bar{W}_f$ from 0.06-0.08 the temperature distribution significantly increases and there onwards from $\bar{W}_f$ = 0.08-0.14 the increase in temperature distribution constantly reduces and becomes nearly equal at 0.12 and 0.14. The fact behind this increase in temperature distribution is that at fixed Reynolds number when the spacing between cells, $\bar{W}_f$, is less the coolant flow velocity increases and when the spacing between cells increases the coolant flow velocity reduces as the criteria of continuity of mass should be satisfied.

At minimum spacing ($\bar{W}_f$ = 0.04) the heat transfer coefficient of coolant increases carrying more heat away from the surface of cell which causes reduced temperature in cell. There are two ways to look at this result obtained: firstly, when $\bar{W}_f$ is reduced from 0.08-0.04 the temperature distribution significantly reduces and then remains almost equal. Hence there exists a lower limiting spacing between the cells below which the temperature reduction is least and only causes more pressure drop. Secondly, when $\bar{W}_f$ is increased from 0.04-0.14 the temperature distribution significantly increases and then again remains very nearly same. Hence there exists an upper limiting spacing between the cells above which the increase in temperature is also least and causes rise in overall size of battery module.

From fig. 4(a)-4(e) it can be seen that with increase in $\zeta_{cc}$ from 0.06-0.10 the decrease in temperature is of similar trend at each $\bar{W}_f$. With increase in $\bar{W}_f$ the temperature increases and with increase in $\zeta_{cc}$ the temperature reduces. According to the definition of $\zeta_{cc}$, mentioned earlier, an increase in $\zeta_{cc}$ at fixed $Ar$ and thermal conductivity of cell means increase in thermal conductivity of coolant which causes more heat dissipation. But it is worth noticing that irrespective of increase or decrease in $\bar{W}_f$, the decrease in temperature with $\zeta_{cc}$ reduces and becomes nearly same for all spacing's at $\zeta_{cc}$ = 0.10. Thus, if $\zeta_{cc}$ is further increased, the decrease/increase in temperature for all spacing's will be negligible. It is worth mentioning at this point that firstly, at any fixed spacing $\bar{W}_f$, with increase in $\zeta_{cc}$ the temperature reduces and becomes nearly same at higher value of $\zeta_{cc}$. Hence there exists an upper limiting value of $\zeta_{cc}$ beyond which the decrease in temperature becomes negligible. The reason behind this heat transfer phenomena is that at fixed $\bar{S}_q$, $\zeta_{cc}$, Re, $Ar$, and $\bar{W}_f$ the heat dissipation from the cell to coolant is limited beyond which it cannot be increased. Secondly, the increase in temperature at $\zeta_{cc}$ = 0.10 with increase in $\bar{W}_f$ is comparatively less. Hence it can be deduced that with further increase in $\zeta_{cc}$ above 0.10 will

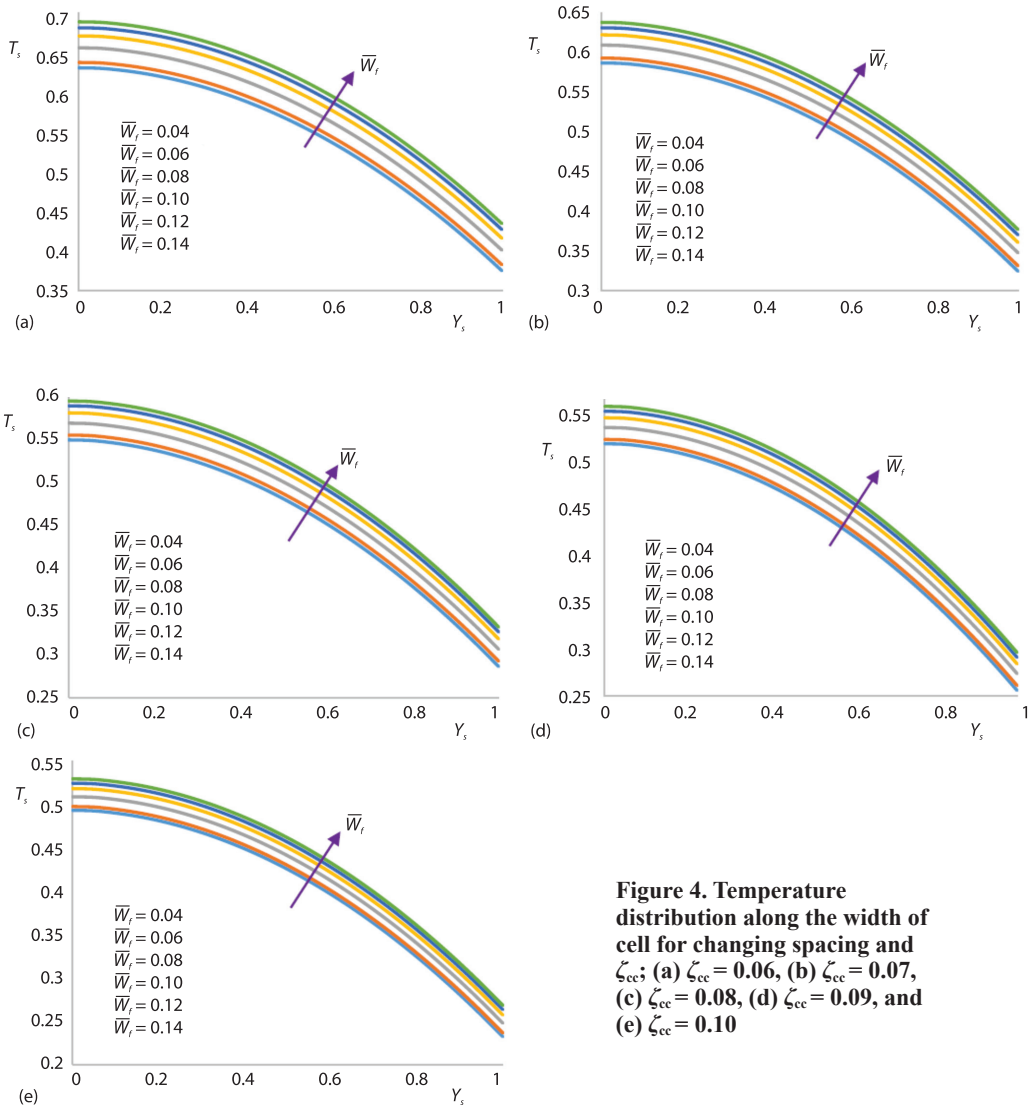


**Figure 4. Temperature distribution along the width of cell for changing spacing and $\zeta_{cc}$; (a) $\zeta_{cc} = 0.06$, (b) $\zeta_{cc} = 0.07$, (c) $\zeta_{cc} = 0.08$, (d) $\zeta_{cc} = 0.09$, and (e) $\zeta_{cc} = 0.10$**

cause negligible decrease in temperature and simultaneous increase in $\overline{W}_f$ will cause negligible increase in temperature. On the other side, if $\zeta_{cc}$ is reduced below 0.06, the temperature in cell increases and may cross its permissible limit causing thermal runaway. Similarly, the spacing between cells cannot be reduced as it causes more pressure drop. Therefore, a lower and an upper limit for both $\zeta_{cc}$ and $\overline{W}_f$ exists below and beyond which it cannot be reduced and increased, respectively.

The variation in temperature distribution of coolant at $X = 0.5$ along the transverse direction with increase in $\overline{W}_f$ is shown in fig. 5. The behavior of temperature distribution in coolant with change in spacing is similar to the effect of spacing shown earlier in fig. 5. For the sake of brevity, figures are not added at different $\zeta_{cc}$ and Reynolds number. The temperature of coolant is least at $\overline{W}_f = 0.04$ and increases with increasing $\overline{W}_f$, however the temperature distribution is monotonous at all spacings. It is noticeable that at lower spacing temperature gradi-

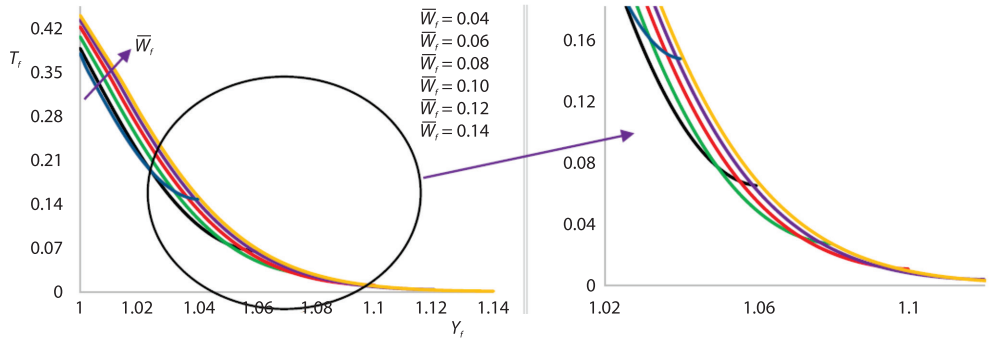


**Figure 5. Fluid temperature distribution in the downstream for changing spacing between the cells**

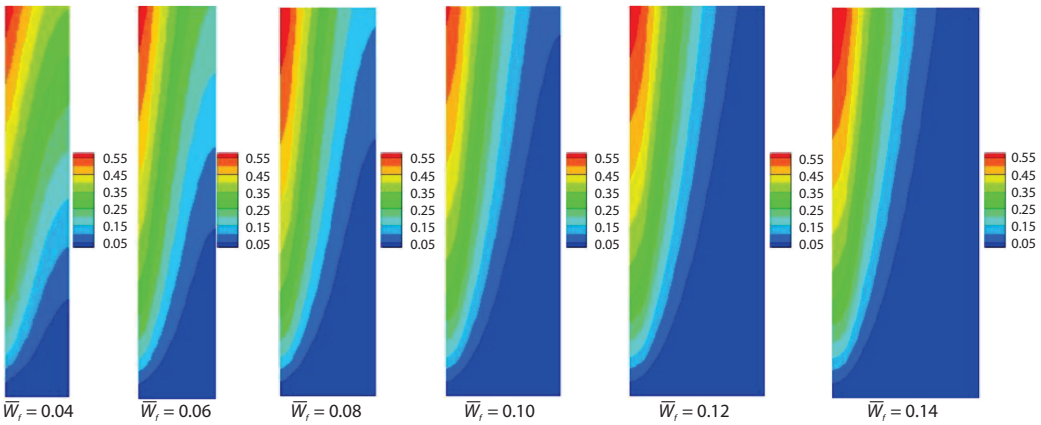


**Figure 6. Temperature contours of coolant for different spacing between cells**

ent is steeper and reduces with increasing spacing. Maximum temperature of coolant is at the trailing edge of the cell and coolant interface and it spreads with spacing as shown in fig. 6. At $\overline{W}_f = 0.04$, the temperature is more uniformly carried by the coolant due to its increased velocity hence the temperature gradient is less. At higher spacings due to decrease in velocity the temperature distribution is mainly concentrated near the surface of cell in stream wise direction and therefore, steeper temperature gradient. The coolant temperature cannot be decreased by merely decreasing the spacing as it causes more pressure drop. Whereas the coolant temperature increases up to a spacing of 0.10 and then remains nearly same on further increase in spacing.

### *Effect of Reynolds numner and spacing on local friction coefficient and Nusselt number*

Figure 7 depicts the variation in local friction coefficient, $C_{f,x}$, at different Renolds number from 250-2000 and when spacing between cells is increased from 0.04-0.14. At all spacings the $C_{f,x}$ is highest for Re = 250 and gradually reduces upto Re = 750. Upon further increases in Re >750, the $C_{f,x}$ remains more or less same and this is true at all spacings considered. The low coolant velocity at Re ≤ 750 causes rapid development of hydrodynamic boundary-layer close to the leading edge of cell hence increased $C_{f,x}$ and there on remains constant near the leading edge. With increase in spacing, the $C_{f,x}$ also reduces for all Reynolds number and remains constant slightly away from the leading edge.

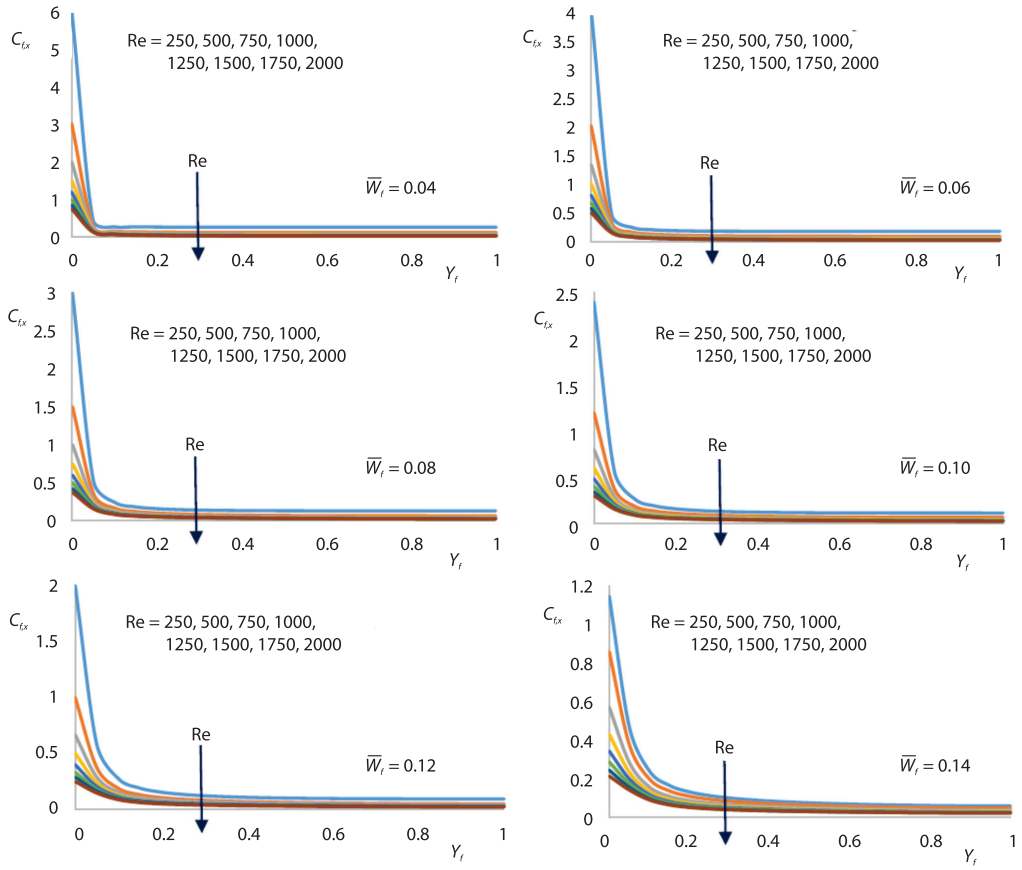


**Figure 7. Local friction coefficient, $C_{f,x}$, at different Reynolds number and spacing, $\overline{W}_f$, between cells**

In fig. 8 the variation of local Nusselt number, $Nu_x$, with increase in spacing between cells and coolant flow Reynolds number is shown. Similar to the effect of Reynolds number and spacing on $C_{f,x}$ shown in fig. 7, $Nu_x$ also increases with increase in Reynolds number and spacing. At low Reynolds number *i.e.* <750, $Nu_x$ is highest at the leading edge where the fluid comes in contact with the cell surface. The $Nu_x$ keeps on reducing along the stream wise direction and becomes constant close to the leading edge. For higher Re and spacings $Nu_x$ smoothly reduces and becomes nearly constant near the trailing edge of cell. Similar trends of $Nu_x$ for increase in Re is reported by Moharana *et al.* in [30].

## Conclusions

In this present work, a realistic conjugate heat transfer analysis of parametric effect on thermal and fluid-flow behavior of battery thermal management system is carried. The effect of few important working parameters like volumetric heat generation, $\overline{S}_q$, conduction-convection parameter, $\zeta_{cc}$, Reynolds number, Aspect ratio, $Ar$, spacing between the cells, $\overline{W}_f$, are studied in this work. Important observations made from detailed analysis are following:

- The conjugate condition adopted indicates the proper selection of coolant flowing over the battery which can significantly regulate its temperature. The conduction-convection param-

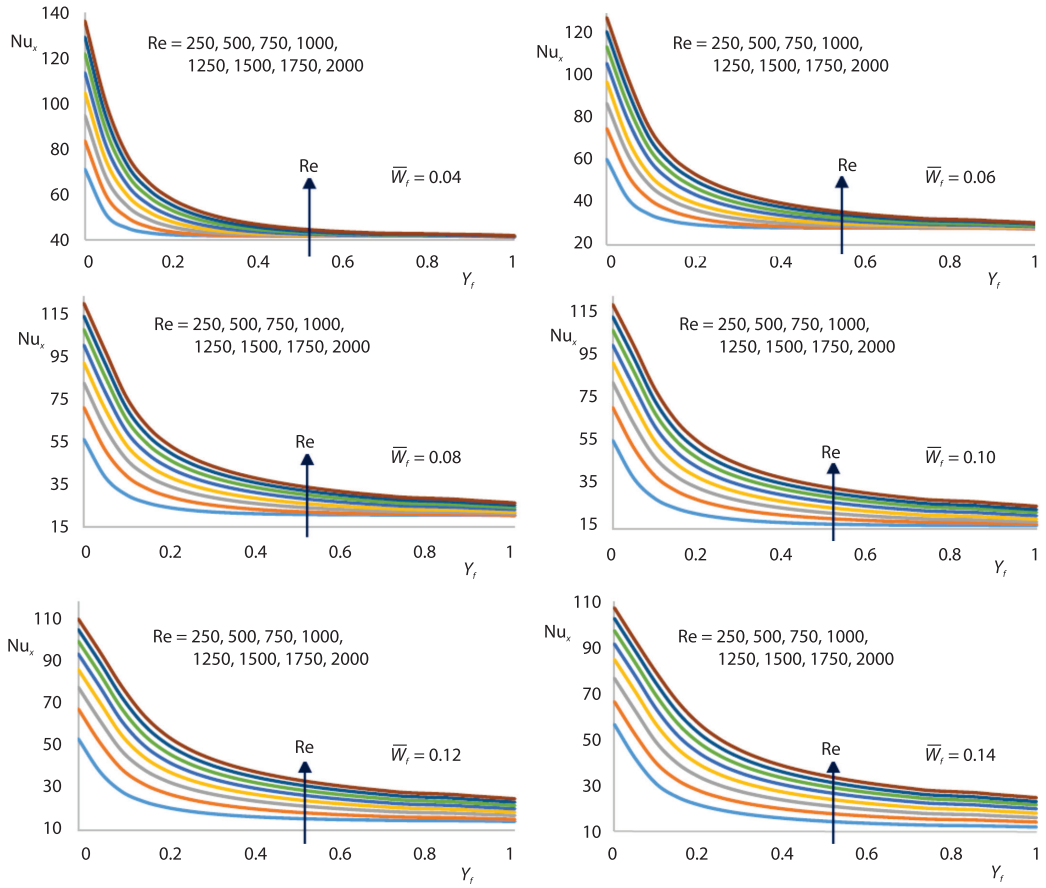


**Figure 8. The $Nu_x$, at different Re and spacing, $\overline{W}_f$, between cells**

eter, arrived in this study dictates the selection of coolant by giving a ratio of thermal conductivity.

- With increase in spacing between the cells the temperature distribution along the width increases up to a certain upper limit as the flow behaves like external flow and the thermal boundary-layers do not mix.
- Simultaneous increase of $\zeta_{cc}$ along with $\overline{W}_f$ causes temperature reduction significantly due to increase of thermal conductivity of fluid.
- The Nusselt number is highest at maximum Reynolds number and also when $\overline{W}_f$ is minimum as the flow mean velocity rises.
- Nusselt number decreases with increase in $\overline{W}_f$ and remains unchanged at higher $\overline{W}_f$ due to thermal boundary-layer being fully developed.
- Friction coefficient is highest at low Reynolds number and $\overline{W}_f$. At maximum Reylonds number, friction coefficient is same for all $\overline{W}_f$.

## Acknowledgment

The authors extend their appreciation the Deanship of Scientific Research at King Khalid University, Abha, Saudi Arabia for funding this work through the Research Group under grant number (R.G.P.1/213/ 41)

## Nomenclature

$Ar$ – aspect ratio of battery cell
$C_f$ – dimensionless friction coefficient transverse direction
$h$ – convective heat transfer coefficient, [$Wm^{-2}k^{-1}$]
$L$ – length of battery cell, [m]
$L_o$ – dimensionless length of extra outlet fluid domain
$L_i$ – dimensionless length of extra inlet fluid domain
$l_o$ – length of extra outlet fluid domain, [m]
$l_i$ – length of extra fluid domain, [m]
$k$ – thermal conductivity, [$Wm^{-1}k^{-1}$]
Nu – Nusselt number
$q'''$ – volumetric heat generation, [$Wm^{-3}$]
$\bar{S}_q$ – dimensionless volumetric heat generation
Pr – Prandtl number
Re – Reynolds number
$T$ – temperature, [°C]
$T_o$ – maximum allowable temperature of battery, [°C]
$\bar{T}$ – non-dimensional temperature
$U$ – non-dimensional velocity along the axial direction
$u$ – velocity along the axial direction, [$ms^{-1}$]
$u_\infty$ – free stream velocity, [$ms^{-1}$]
$V$ – non-dimensional velocity along the
$v$ – velocity along the transverse direction, [$ms^{-1}$]
$\bar{W}$ – non-dimensional width
$w$ – half width, [m]
$X$ – non-dimensional axial direction
$x$ – axial direction
$Y$ – non-dimensional transverse direction
$y$ – transverse direction

### *Greek symbols*

$\alpha$ – thermal diffusivity of fluid, [$m^2s^{-1}$]
$\nu$ – kinematic viscosity of fluid, [$m^2s^{-1}$]
$\rho$ – density of fluid, [$kgm^{-3}$]
$\zeta_{cc}$ – conduction-convection parameter
$\mu$ – dynamic viscosity, [$Nm^2s^{-1}$]

### *Subscripts*

f – fluid domain
avg – average
s – solid domain (battery cell)
$\infty$ – free stream
m – mean

## References

[1] Feng, X., *et al*., Thermal Runaway Mechanism of Lithium Ion Battery for Electric Vehicles: A Review, *Energy Storage Mater*., *10* (2018), Jan., pp. 246-267
[2] A. Nazari, A., Farhad, S., Heat Generation in Lithium-Ion Batteries with Different Nominal Capacities and Chemistries, *Appl. Therm. Eng*., *125* (2017), Oct., pp. 1501-1517
[3] Bandhauer, T. M., *et al.,* A Critical Review of Thermal Issues in Lithium-Ion Batteries, *Journal Electrochem. Soc*., *158* (2011), 3, pp. R1-R25
[4] Zhao, R., *et al.,* Simulation and Experimental Study on Lithium Ion Battery Short Circuit, *Appl. Energy*, *173* (2016), July, pp. 29-39
[5] Ye, J., *et al.,* Thermal Behavior and Failure Mechanism of Lithium Ion Cells during Overcharge under Adiabatic Conditions, *Appl. Energy*, *182* (2016), Nov., pp. 464-474
[6] Peng, P., Jiang, F., Thermal Safety of Lithium-Ion Batteries with Various Cathode Materials: A Numerical Study, *Int. J. Heat Mass Transf*., *103* (2016), Dec., pp. 1008-1016
[7] Thankgod, E. B., *et al.*, Carbon Nanotubes: Building Blocks of Nanotechnology Development, *Journal Nanotech. Prog. Int.*, *6* (2016), 2
[8] Layeni, A., *et al., Computational Analysis of a Lecture Room Ventilation System*, IntechOpen, Rijeka, Croatia, 2020
[9] Baker, D., Verbrugge, M. W., Temperature and Current Distribution in Thin-Film Batteries, *Journal Electrochem. Soc*., *146* (1999), 7, pp. 2413-2424
[10] Ramadass, P., Capacity Fade of Li – Ion Cells Cycled at Elevated Temperatures, *Journal Power Sources*, *112* (2002), 2, pp. 606-613
[11] Mahamud, R., Park, C., Reciprocating Air-Flow for Li-Ion Battery Thermal Management to Improve Temperature Uniformity, *Journal Power Sources*, *196* (2011), 13, pp. 5685-5696
[12] Tran, T., *et al.,* Experimental Investigation on Heat Pipe Cooling for Hybrid Electric Vehicle and Electric Vehicle Lithium-Ion Battery, *Journal Power Sources*, *265* (2014), Nov., pp. 262-272
[13] Salman Ahmed, S., *et al.,* Effect of Viscous Dissipation on Aiding Flow Heat and Mass Transfer in Porous Cavity, *AIP Conf. Proc*., *2104* (2019), 1, 030055
[14] Ameer Ahamad, A. R., *et al.,* Heat Transfer in a Porous Cavity with an Internal Heating Strip Towards Cold Surface., *Mater. Today Proc*., *27* (2019), 2, pp. 1863-1863

[15] Rao, Z., *et al.,* Thermal Performance of Liquid Cooling Based Thermal Management System for Cylindrical Lithium-Ion Battery Module with Variable Contact Surface, *Appl. Therm. Eng*., *123* (2017), Aug., pp. 1514-1522
[16] Chen, D., *et al.,* Comparison of Different Cooling Methods for Lithium Ion Battery Cells, *Appl. Therm. Eng*., *94* (2016), Feb., pp. 846-854
[17] Basu, S., *et al.,* Coupled Electrochemical Thermal Modelling of a Novel Li-Ion Battery Pack Thermal Management System, *Appl. Energy*, *181* (2016), Nov., pp. 1-13
[18] Chalise, D., *et al.,* Conjugate Heat Transfer Analysis of Air/Liquid Cooling of a Li-Ion Battery Pack, *Journal Electrochem. Energy Convers. Storage*, *15* (2018), 011008, pp. 1-8
[19] Li, X., *et al.,* Thermal Management of Cylindrical Batteries Investigated Using Wind Tunnel Testing and Computational Fluid Dynamics Simulation, *Journal Power Sources*, *238* (2013), Sept., pp. 395-402
[20] Afzal, A., *et al.,* Steady and Transient State Analyses on Conjugate Laminar Forced Convection Heat Transfer, *Arch. Comput. Methods Eng*., *27* (2020), Jan., pp. 135-170
[21] Afzal, A., *et al.,* Thermal Management of Modern Electric Vehicle Battery Systems (MEVBS), *Journal Therm. Anal. Calorim*., *144* (2020), Apr., pp. 1271-1295
[22] Mokashi, I., *et al.,* Maximum Temperature Analysis in a Li-Ion Battery Pack Cooled by Different Fluids, *Journal Therm. Anal. Calorim*., *141* (2020), Aug., pp. 2555-2571
[23] Afzal, A., *et al.,* Effect of Spacing on Thermal Performance Characteristics of Li-Ion Battery Cells, *Journal Therm. Anal. Calorim*., *135* (2019), 3, pp. 1797-1811, 2019
[24] Karimi, G., Li, X., Thermal Management of Lithium-Ion Batteries for Electric Vehicles, *Int. J. Energy* Res., *37* (2012), 1, pp. 13-24
[25] Pinto, R., *et al.,* Computational Fluid Dynamics in Turbomachinery: A Review of State of the Art, *Arch. Comput. Methods Eng*., *24* (2017), 3, pp. 467-479
[26] Afzal, A., *et al.,* Parallelization Strategies for Computational Fluid Dynamics Software: State of the Art Review, *Arch. Comput. Methods Eng*., *24* (2017), 2, pp. 337-363
[27] Yu, K., *et al.,* Thermal Analysis and Two-Directional Air-Flow Thermal Management for Lithium-Ion Battery Pack, *Journal Power Sources*, *270* (2014), Dec., pp. 193-200
[28] Jahangeer, S., *et al.,* Conjugate Heat Transfer Analysis of a Heat Generating Vertical Plate, *Int. J. Heat Mass Transf*., *50* (2007), 1-2, pp. 85-93
[29] Ramis, M. K., *et al.,* Conjugate Conduction-Forced Convection Heat Transfer Analysis of a Rectangular Nuclear Fuel Element with Non-Uniform Volumetric Energy Generation, *Int. J. Heat Mass Transf*., *51* (2008), 3-4, pp. 517-525
[30] Moharana, M. K., *et al.,* Optimum Nusselt Number for Simultaneously Developing Internal Flow under Conjugate Conditions in a Square Micro-Channel, *Journal Heat Transfer*, 134 (20212), 7, 071703

Paper submitted: December 6, 2019
Paper revised: August 29, 2020
Paper accepted: September 2, 2020